Microwave magnetoelectric coupling and ferromagnetic resonance frequency tuning of a Co_2MnSb/GaAs/PZN-PT heterostructure

Yajie Chen,[1,*] Aria Yang,[1] Moti R. Paudel,[2,†] Shane Stadler,[2] C. Vittoria,[1] and V. G. Harris[1]

[1]*Center for Microwave Magnetic Materials and Integrated Circuits and the Department of Electrical and Computer Engineering, Northeastern University, Boston, Massachusetts 02115, USA*

[2]*Department of Physics & Astronomy, Louisiana State University, Baton Rouge, Louisiana 70803, USA*

(Received 2 September 2010; revised manuscript received 26 January 2011; published 14 March 2011)

A systematic study of electric-field-tuned ferromagnetic resonance (FMR) of a ferroelectric/ferromagnetic/semiconductor multiferroic heterostructure, consisting of a Co_2MnSb epitaxial film grown on a GaAs substrate bonded to a lead zinc niobate–lead titanate crystal, is reported. The films, grown by pulsed laser deposition, were studied for their crystallographic structure, magnetocrystalline anisotropy, and magnetostrictive and ferromagnetic resonance properties. Ferromagnetic resonance measurements were carried out at *X*-band frequency under the application of electric fields with external magnetic fields applied along the [110], [100], [1$\bar{1}$0], and [001] directions of the Heusler film. Magnetic anisotropy fields were derived from the angular dependence of FMR measurements, yielding an in-plane fourth-order anisotropy constant $K_1 = -150 \times 10^3$ erg/cm^3 and a perpendicular second-order anisotropy constant $K_\perp = 12 \times 10^3$ erg/cm^3. A theoretical model, which includes the effects of electric-field tuning, is presented to calculate the tunability of the ferromagnetic resonance frequency of the multiferroic heterostructure. The multiferroic heterostructure exhibits a frequency tuning of 450 MHz under the application of an electric field of 10 kV cm^{-1}, corresponding to a magnetoelectric coupling coefficient of 8.8 Oe cm kV^{-1}. This work explores the potential of electronically controlled multiferroic devices for use in microwave integrated circuits, while concomitantly establishing the basic theoretical foundation allowing for the calculation of microwave tunability for this and other heterostructures.

DOI: 10.1103/PhysRevB.83.104406 PACS number(s): 75.85.+t, 75.80.+q, 76.50.+g, 77.65.−j

I. INTRODUCTION

Multiferroic (MF) materials exhibiting the magnetoelectric (ME) effect have recently drawn attention for their fundamental physical behavior as well as for their potential in a new class of magnetoelectric devices.[1,2] Among the numerous investigations appearing in the literature, multiferroic metamaterials, constructed as multilayered or granular heterostructures, have drawn the most attention.[3] Multiferroic heterostructures have indeed been shown to offer unique opportunities in the development of many new multifunctional devices, including electric-field-controlled (EFC) magnetic memory elements,[4–6] EFC microwave devices,[7] and *E*- and *H*-field transducers having magnetically modulated piezoelectricity or electrically modulated magnetoelectricity.[8,10] In many of these examples, mechanical coupling between piezoelectric and magnetostrictive layers provides electrical control of magnetic properties of the magnetostrictive layer(s). In contrast, Geiler *et al.*[11] have demonstrated the generation of external fringe fields by MF heterostructures that act on nearby microwave devices that are decoupled from the MF heterostructure. In both instances the MF heterostructures eliminate the need for voluminous and costly magnetic-field coils to actively tune magnetic components. These developments represent a disruptive advance in the field of multifunctional electronics.

Although recent studies have made progress in the application of MF materials and the magnetoelectric effect in the above-mentioned technologies, little work has been performed in introducing these novel materials to microwave integrated circuits (MICs), which are widely used in, among other applications, satellite systems that require smaller, lighter, power-efficient, and less expensive circuits or when the parasitic reactance inherent to hybrid integrated circuits degrades circuit performance. The latter typically occurs in the upper-microwave- and millimeter-wave frequency bands. In these situations, GaAs MICs offer substantial advantages over others, including enhanced system performance from the inclusion of multifunctionality (e.g., rf and logic) in a single circuit, enhanced reproducibility from uniform processing and integration of all parts of the circuit, and wider frequency-bandwidth performance deriving from the reduction of parasitic reactance in discrete device packages, among other benefits.[12] To our knowledge, studies of multifunctional integrated technology, especially those combined with multiferroic heterostrutures, have been few.[13,14] We put forward here the suggestion that multiferroic systems based on semiconductor substrates would potentially lead to on-chip integration of important components such as microwave field-effect transistors (FETs), etc., where the enhancement of coupling efficiency between ferroelectric and ferromagnetic layers would enable significant reduction in dimensionality while improving the performance of microwave circuits.

Many Heusler alloys, such as Co_2MnAl, Co_2MnSi, Co_2MnGe, etc.,[15–19] are predicted to be half metals, defined as having all conducting electrons existing in one spin state. Such a property provides, in theory, infinite gain and spin transport efficiency for such applications as source, drain, or gate materials in spin FETs and other spintronic devices.[20] The present work focuses on exploring new opportunities, such as microwave magnetic semiconductor integrated devices, for this class of Heusler alloy films in combination with the magnetoelectric effect. Here, we aim to demonstrate the electric-field tunability of microwave properties of a

 ©2011 American Physical Society

ferroelectric/ferromagnetic/semiconductor sandwich structure consisting of a ferromagnetic Co_2MnSb alloy film epitaxially grown on a GaAs substrate and bonded to ferroelectric lead zinc niobate–lead titanate (PZN-PT). Since Heusler films of this type have moderate to low ferromagnetic resonance (FMR) linewidths, 100–200 Oe at X-band frequencies,[21] such structures may find application in microwave devices. A key component of the present study is an expanded model put forth to describe and predict the FMR behavior of such structures under application of an external electric field applied across the ferroelectric element.

II. THEORETICAL MODEL OF FMR FOR MF HETEROSTRUCTURES

In order to describe the electric-field tuning of ferromagnetic resonance in a Co_2MnSb/GaAs/PZN-PT heterostructure, we first present and discuss the theoretical formulation of FMR for a Heusler film, such as Co_2MnSb. This will be done for resonance conditions corresponding to the principal field orientations, i.e., for the dc field H applied normal to the sample plane, or within the sample plane along high-symmetry crystallographic directions.[22] We apply the well-known Landau-Lifshitz-Gilbert equation for precession of magnetization to describe the dynamics of FMR in the Co_2MnSb film. We begin with the expression for the free-energy density F in an applied dc magnetic field H for a cubic Co_2MnSb film. Subsequently, the E-field-induced magnetic field will be introduced into the formulism to establish a basic equation enabling one to describe the general case of E-field microwave tunability of FMR in MF heterostructures of this type.

A. FMR of Heusler films

During ferromagnetic resonance, the precession of magnetic moments with free energy $F(\theta,\varphi)$ occurs at a frequency given by[23]

$$\left(\frac{f}{\gamma'}\right)^2 = \frac{1}{M^2\sin^2\theta_0}\left[\frac{\partial^2 F}{\partial\theta^2}\frac{\partial^2 F}{\partial\varphi^2} - \left(\frac{\partial^2 F}{\partial\theta\,\partial\varphi}\right)\right], \qquad (1)$$

where $\gamma\prime = \gamma/2\pi$ [the gyromagnetic ratio $\gamma = g(e/2mc)$], θ and φ are the polar and azimuth angles of $\mathbf{M}$, θ_0 is the equilibrium angle of θ at resonance, and f is the operating frequency. F stands for the total magnetic free-energy density. The relationships between magnetization and applied magnetic field with respect to the film's crystallographic axes are illustrated in Fig. 1. Since the resonance frequency is related to the second derivatives of F, it is essentially a measure of the "curvature" of F, or in a physical sense the "stiffness" of M in response to the applied magnetic field. If the magnetization is oriented along a minimum, or "easy" direction of the added energy, the curvature of F is increased, and the applied field needed to make the resonance frequency equal to the pumping frequency, H_r, is decreased. Similarly, if the magnetization is oriented along a "hard" direction of the added energy, H_r is increased. An increased value of H_r corresponds to a hard direction and a decreased value of H_r corresponds to an easy direction.

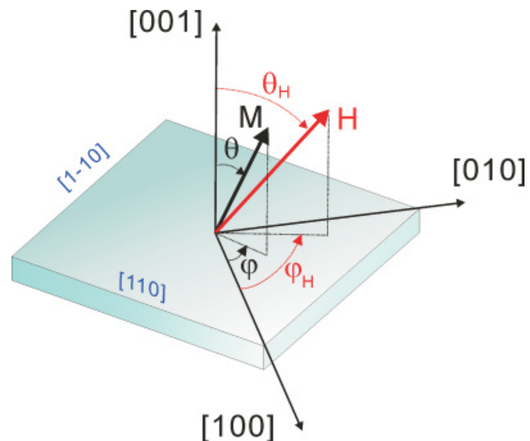

FIG. 1. (Color online) Coordinate system used in this work that describes the orientation of the dc magnetic field H and resulting equilibrium orientation of the magnetization M with respect to the crystallographic orientation of the Co_2MnSb films.

Ferromagnetic resonance data generally vary with an applied field within the plane of the film due to in-plane magnetic anisotropy. Interestingly, the measured FMR data lack the fourfold symmetry expected to appear in the (001) plane of cubic magnetic materials, such as the class of Heusler films under consideration. Specifically, there is likely a pronounced difference between the anisotropy energy along the two [110] directions while the in-plane [100] directions remain largely unchanged.[24] Therefore, the total energy can be expressed by

$$F = K_1\left(\alpha_1^2\alpha_2^2 + \alpha_2^2\alpha_3^2 + \alpha_3^2\alpha_1^2\right) + 2\pi M_\perp^2 - \mathbf{M}\cdot\mathbf{H} - K_\perp\cos^2\theta - K_u\sin^2\theta\cos^2(\varphi - \pi/4), \qquad (2)$$

where K_1 is the fourth-order crystalline cubic anisotropy with α_i being the direction cosines of $\mathbf{M}$ in the cubic axes, $K_\perp$ is a second-order anisotropy term normal to the film, and the second-order K_u anisotropy term is included to represent the inequivalence between [110] and $[1\bar{1}0]$. Here, it is assumed that the K_u axis aligns along [110]. Note that the second and third terms on the right-hand side of Eq. (2) represent the shape anisotropy energy (or demagnetizing energy) and the Zeeman energy, respectively. These two types of anisotropy, i.e., cubic and uniaxial, arise from the crystal structure of the material. The perpendicular and in-plane cubic and perpendicular uniaxial anisotropy terms are usually considered to be due to the strain in the crystal lattice caused by the lattice constant mismatch between the Co_2MnSb film and the substrate on which it was grown.[25] The in-plane uniaxial term is due to the fact that there is a difference between the [110] and $[1\bar{1}0]$ crystallographic directions despite the high-symmetry zinc-blende structure of the material.[26] Heinrich *et al.*[27,28] have recently found an alternative mechanism of in-plane or perpendicular magnetic anisotropy in Heusler alloys related to ordered lattice defects which are more pronounced in thick films, such as epitaxially grown NiMnSb(001) films grown on an InGaAs/InP(001) template.

The resonance condition for any given field orientation is derived from Eqs. (1) and (2) by minimizing the free energy F with respect to θ and φ. Here, we describe the FMR conditions with the external magnetic field H aligned along the four main crystallographic axes. For the (001) plane, the FMR equilibrium equations can be expressed as

$$\left(\frac{f}{\gamma'}\right)^2 = \left[H\cos(\varphi-\varphi_H) + 4\pi M - \frac{2K_\perp}{M} + \frac{K_1}{M}(2-\sin^2 2\varphi) + \frac{2K_u}{M}\cos^2(\varphi-\pi/4)\right] \times \left[H\cos(\varphi-\varphi_H) + \frac{2K_1}{M}\cos 4\varphi + \frac{2K_u}{M}\cos 2(\varphi-\pi/4)\right], \quad (3)$$

for $\theta=\theta_H=90^\circ$ and $\varphi=\varphi_H=45^\circ$, **M** and **H** parallel to [110], i.e., parallel to the film plane,

$$\left(\frac{f}{\gamma'}\right)^2 = \left(H_r - \frac{2K_1}{M} + \frac{2K_u}{M}\right) \times \left(H_r + 4\pi M - \frac{2K_\perp}{M} + \frac{K_1}{M} + \frac{2K_u}{M}\right), \quad (4)$$

for $\theta=\theta_H=90^\circ$ and $\varphi=\varphi_H=-45^\circ$, **M** and **H** parallel to $[1\bar{1}0]$, i.e., parallel to the film plane,

$$\left(\frac{f}{\gamma'}\right)^2 = \left(H_r - \frac{2K_1}{M} - \frac{2K_u}{M}\right) \times \left(H_r + 4\pi M - \frac{2K_\perp}{M} + \frac{K_1}{M}\right), \quad (5)$$

and, for $\theta=\theta_H=90^\circ$ and $\varphi=\varphi_H=0^\circ$, **M** and **H** parallel to [100], i.e., parallel to the film plane,

$$\left(\frac{f}{\gamma'}\right)^2 = \left(H_r + \frac{2K_1}{M}\right) \times \left(H_r + 4\pi M - \frac{2K_\perp}{M} + \frac{K_u}{M} + \frac{2K_1}{M}\right). \quad (6)$$

In order to obtain the FMR condition for **H** aligned along [001], we consider **M** and **H** within the $(1\bar{1}0)$ plane, i.e., $\varphi=\varphi_H=\pi/4$. Thus, we can write the expression

$$\left(\frac{f}{\gamma'}\right)^2 = \left[H_r\cos(\theta-\theta_H) + \left(-4\pi M + \frac{2K_\perp}{M} + \frac{K_1}{2M}\right)\cos 2\theta + \frac{3K_1}{2M}\cos 4\theta + \frac{2K_u}{M}\right] \times \left[H_r\cos(\theta-\theta_H) + \left(-4\pi M + \frac{2K_\perp}{M} + \frac{K_1}{2M}\right)\cos^2\theta + \frac{3K_1}{2M}\cos 4\theta - \frac{2K_1}{M}\right]. \quad (7)$$

For $\theta=\theta_H=0^\circ$, **M** and **H** parallel to [001], i.e., perpendicular to the film plane,

$$\left(\frac{f}{\gamma'}\right)^2 = \left(H_r - 4\pi M + \frac{2(K_\perp + K_1 - K_u)}{M}\right) \times \left(H_r - 4\pi M + \frac{2(K_\perp + K_1)}{M}\right). \quad (8)$$

B. Ferromagnetic resonance under application of an electric field across the multiferroic heterostructure

We assume that the configuration of fields within this heterostructure is as illustrated in Fig. 2. The measurements are performed for two cases in which the electric field is applied perpendicular to the PZN-PT crystal. The first case is when the applied magnetic field is aligned along the d_{32} direction of PZN-PT crystal, corresponding to the [110] direction of the Heusler film. The second is for an applied magnetic field aligned along the d_{31} direction of the PZN-PT crystal, corresponding to $[1\bar{1}0]$ of the magnetic film. Note that the stress-induced magnetic field is determined by the electromechanical coefficient d_{31} (or d_{32}) and the magnetostrictive coefficient (λ) in a reference direction. In this case, an electric-field-induced magnetic field mediated by a strain always aligns along d_{32} whether an external magnetic field lies along the d_{31} or d_{32} direction (we ignore the possible cone configuration of the induced field).[29]

Since the induced magnetic field is restricted to lie in the film plane (001) and aligns along the [110] direction, the stress-induced energy is written as

$$F_\sigma^E = -K_\sigma^E \sin^2\theta\cos^2(\varphi-\pi/4), \quad (9)$$

where K_σ^E is a stress-induced magnetic anisotropy constant. Therefore, the induced uniaxial anisotropy generated by an applied electric field must be included in Eq. (2). Combining Eqs. (2) and (7), the FMR equilibrium condition in the (001)

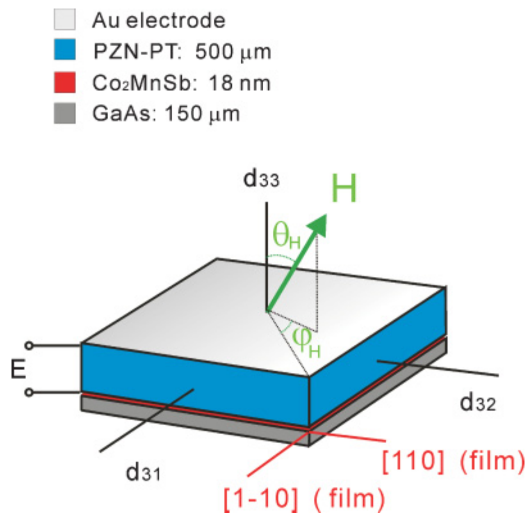

FIG. 2. (Color online) Schematic diagram depicting the H and E fields within the Co_2MnSb/GaAs/PZN-PT multiferroic heterostructure.

plane, i.e., $\theta=\pi/2$, under application of electric field can be expressed as

$$\left(\frac{f}{\gamma'}\right)^2 = \left[H_r \cos(\varphi-\varphi_H) + 4\pi M - \frac{2K_\perp}{M} + \frac{K_1}{M}(2-\sin^2 2\varphi) + \frac{2K_u}{M}\cos^2\left(\varphi-\frac{\pi}{4}\right) + \frac{2K_\sigma^E}{M}\cos^2\left(\varphi-\frac{\pi}{4}\right)\right] \times\left[H_r\cos(\varphi-\varphi_H) + \frac{2K_1}{M}\cos 4\varphi + \frac{2K_u}{M}\cos 2\left(\varphi-\frac{\pi}{4}\right) + \frac{2K_\sigma^E}{M}\cos 2\left(\varphi-\frac{\pi}{4}\right)\right]. \quad (10)$$

We now rewrite the ferromagnetic resonance conditions for two directions of the applied electric field. When a magnetic field is aligned along d_{32} of the PZN-PT crystal, and **M** and **H** align along the [110] direction of the Co_2MnSb film, i.e., **H**//[110], $\varphi=\pi/4$, the resonance condition can be expressed as[30]

$$\left(\frac{f}{\gamma'}\right)^2 = \left(H_r + \frac{2K_\sigma^E}{M} + \frac{2K_u}{M} - \frac{2K_1}{M}\right) \times\left(H_r + 4\pi M + \frac{2K_\sigma^E}{M} + \frac{2K_u}{M} - \frac{2K_\perp}{M} + \frac{K_1}{M}\right). \quad (11)$$

When a magnetic field is aligned along d_{31} of the PMN-PT crystal, and **M** and **H** align along the $[1\bar{1}0]$ direction of the Co_2MnSb film, i.e., **H**//$[1\bar{1}0]$, $\varphi=-\pi/4$, the external magnetic field is transverse to the induced uniaxial anisotropy field. Thus, we obtain

$$\left(\frac{f}{\gamma'}\right)^2 = \left(H_r - \frac{2K_\sigma^E}{M} - \frac{2K_u}{M} - \frac{2K_1}{M}\right) \times\left(H_r + 4\pi M - \frac{2K_\perp}{M} + \frac{K_1}{M}\right). \quad (12)$$

III. EXPERIMENTAL DETAILS

A Co_2MnSb film was epitaxially grown on a GaAs (001) substrate by pulsed laser deposition (PLD) in an ultrahigh-vacuum chamber having a base pressure less than 10^{-8} Torr and a substrate temperature of 450 K. The deposition source was a KrF (λ=248 nm) excimer laser with a 20 ns pulse duration at a 10 Hz repetition rate. The deposition rates were monitored with a quartz crystal monitor calibrated using Rutherford backscattering spectroscopy (RBS). RBS was also used to measure the stoichiometry of both the targets and film samples. Here, samples were grown with overall deposition rates of ~20 Å/min and thicknesses of 180 Å ± ~5%. The film phase was identified through x-ray diffraction (XRD) measurements at room temperature using a Rigaku U3 x-ray diffractometer employing Cu $K\alpha$ radiation. Representative data are presented in Fig. 3. XRD analysis indicates a single-phase (001)-textured epitaxial film of $L2_1$ structure with lattice parameters $a=b=c=6.021$ Å on a GaAs substrate with $a=5.6568$ Å. Additionally, the thickness of the film was further confirmed to be 184 ± 29 Å by application of the Scherrer analysis using $B(2\theta)=\frac{0.94\lambda}{L\cos\theta}$, where $B(2\theta)$ is the full width in radians subtended by the half-maximum-intensity width of the diffraction peak and L is the vertical depth of the crystal plane. This result is in relative agreement with the results derived from RBS. The compositional analysis was done with RBS, and confirmed using x-ray fluorescence (XRF) spectroscopic measurements, indicating a film composition of $Co_2Mn_{0.92}Sb_{0.42}$. A more extensive description of the growth conditions have been published elsewhere.[31,32]

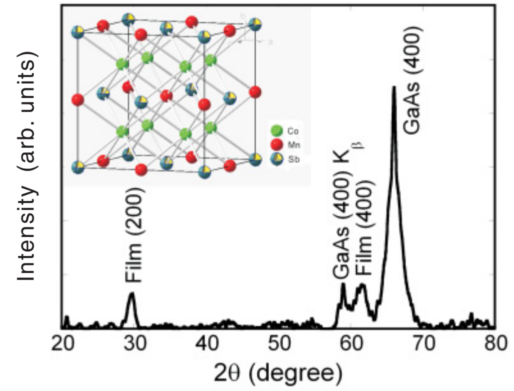

FIG. 3. (Color online) XRD spectrum of Co_2MnSb film. Inset illustrates an $L2_1$-type structure.

Static magnetic properties were measured using vibrating sample magnetometry (VSM; Lakeshore Model 7400). The magnetostriction constant (λ) was measured using a high-precision optical technique over a magnetic field range of 0–250 Oe. Ferromagnetic resonance measurements were carried out using a microwave cavity excited in a TE_{102} mode at X-band frequency ($f=9.55$ GHz).

To produce strong ME coupling in the MF heterostructure it was crucial to select a high-functioning piezoelectric crystal as the substrate.[33] A relaxor-based ferroelectric single crystal, $Pb(Zn_{1/3}Nb_{2/3})O_3$–$PbTiO_3$, consisting of a rhombohedral symmetric PZN and a tetragonal-symmetry ferroelectric, lead titanate (PT), was chosen. This crystal features exceptional dielectric and electromechanical properties: e.g., $k_{33}=0.86$,

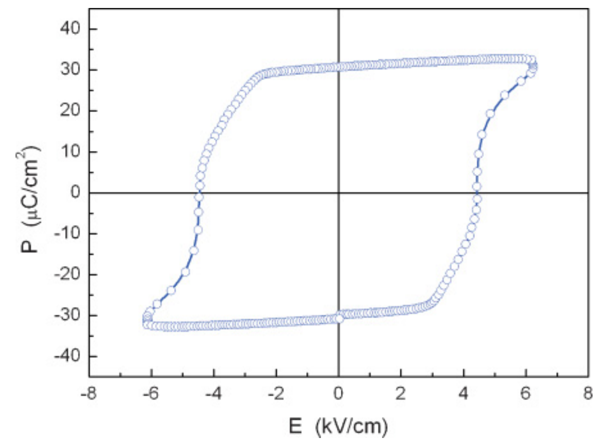

FIG. 4. (Color online) Dependence of polarization upon electric-field strength for the PZN-PT crystal used in the heterostructure of the present study.

$d_{32} = 1100$ pC/N, $d_{31} = -2700$ to -3200 pC/N, $d_{33} = 1500$ pC/N, $K^T > 5000$, and $\tan\delta < 0.01$ at 1 kHz.[34] These electromechanical properties are superior to those of other ferroelectric crystals such as $Pb(Mg_{1/3}Nb_{2/3})O_3$–$PbTiO_3$ (PMN-PT), which is commonly used in similar MF heterostructures.[35,36] In the present work, the PZN-PT crystal is (011) cut and [011] poled with anisotropic in-plane piezoelectric coefficients $d_{31} = -2800$ pC/N and $d_{32} = 1100$ pC/N. The electric-field dependence of the electronic polarization was measured by a ferroelectric measurement system (Radiant Technologies, Inc.). The GaAs substrate was thinned by mechanical polishing to 150 μm before being bonded to the PZN-PT crystal. The multiferroic heterostructure was designed to operate in the longitudinal magnetized–transverse polarized mode. The PZN-PT slab and Co_2MnSb film on GaAs substrate were bonded with a quick-curing ethyl cyanoacrylate adhesive. Magnetoelectric coupling measurements were carried out in which **H** was alternately aligned parallel to the d_{31} and d_{32} directions of the PZN-PT crystal. Applied voltages ranged from -400 to 400 V across the PZN-PT crystal, corresponding to an electric-field strength E of -8 to $+8$ kV/cm. Figure 4 presents a correlation of electronic polarization (P) to electric field for the PZN-PT crystal. Generally, the existence of the P-E loop is considered evidence supporting ferroelectricity. It is pointed out that a polarization switching leads to strain—electric-field hysteresis. A typical strain—field-response curve is often referred to as the "butterfly loop." As the electric field is applied, the converse piezoelectric effect dictates that a strain results. As the field is increased, the strain is no longer linear with the field as domain walls nucleate and begin to coalesce. The characteristics have a direct influence on the behavior of the magnetoelectric coupling in the heterostructure.

IV. RESULTS AND DISCUSSION

A. Static magnetic properties

Figure 5 presents magnetic hysteresis loops for Co_2MnSb films when an external H field is applied along different directions in the (001) plane. Note that the measurement

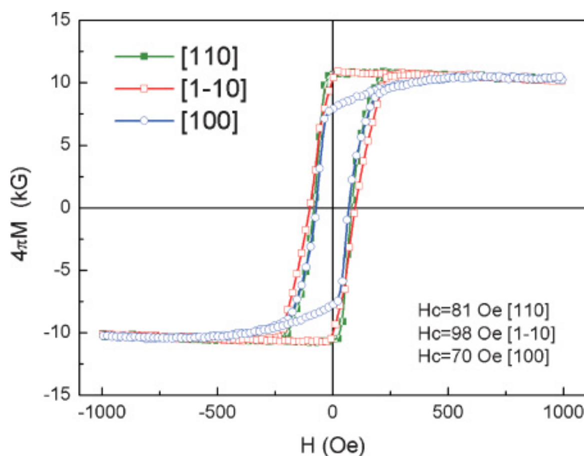

FIG. 5. (Color online) Magnetic hysteresis loops of Co_2MnSb film magnetized along different crystal axes. The diamagnetic slope in each curve originates from the GaAs substrates (see text).

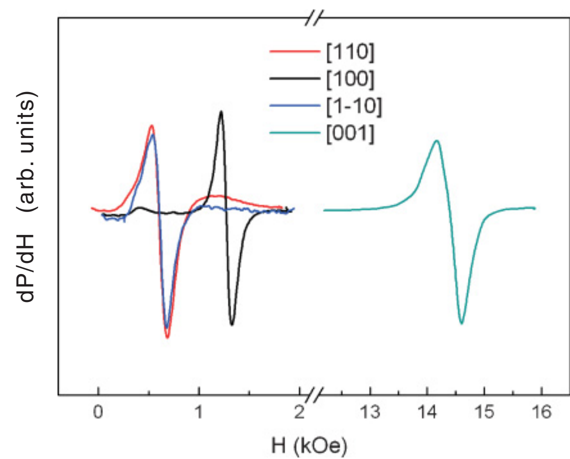

FIG. 6. (Color online) FMR spectra collected along different crystallographic directions for a 180-Å-thick Co_2MnSb film.

indicates magnetic easy axes existing along [110] and [1$\bar{1}$0], while [100] represents the hard axis. The film shows coercivity and remanant magnetization values of $H_c = 90$ Oe, $4\pi M_r = 10.57$ kG ([110]); 67 Oe, 10.12 kG ([1$\bar{1}$0]); and 50 Oe, 8.015 kG ([100]). A saturation magnetization ($4\pi M_s$) of 10.8 kG was measured, consistent with phase purity and accurate film composition. The magnetization values along the [110] and [1$\bar{1}$0] directions illustrate a slight difference, which is in contrast to the substantial differences previously reported.[37] This observation is attributed to the unique composition and thickness of the films of the present study compared with those of Refs. 28 and 29. Note that all of the magnetic hysteresis loops contain a diamagnetic contribution arising from the GaAs substrates. The magnetostrictive measurement indicates that the Co_2MnSb film has a saturation magnetostrictive coefficient λ_s of 11 ppm, which is comparable to values previously reported for Heusler alloys.[38]

B. Ferromagnetic resonance properties

Some recent experiments[26] indicate that the spin relaxation in Heusler compounds, i.e., the Gilbert damping constant, is comparable to or lower than that in other magnetic metals, such as Permalloy.[39] Because of this, Heusler alloys possess unique potential for use in high-frequency devices. In the present work, FMR measurements were carried out for the magnetic film along the four major crystallographic axes. These results are presented in Fig. 6. For $\theta{=}\theta_H = 90^\circ$ and $\varphi_H{=}45^\circ$, **M** and **H** parallel to [110], i.e., parallel to the film plane, the resonance field and linewidth are $H_{r[110]} = 0.610$ kOe and 130 Oe, respectively. The measurement along the [1$\bar{1}$0] direction shows similar results to those of the [110] direction, i.e., H_r,[1$\bar{1}$0]=0.616 kOe and ΔH=150 Oe. For $\theta{=}\theta_H{=}90^\circ$ and $\varphi_H{=}0^\circ$, **M** and **H** parallel to [100], i.e., parallel to the film plane, $H_{r,[100]} = 1.268$ kOe and $\Delta H = 110$ Oe. For $\theta{=}\theta_H = 0^\circ$, **M** and **H** parallel to [100], i.e., perpendicular to the film plane, $H_{r,[001]}$ is 14.40 kOe with a corresponding linewidth of 380 Oe. It is known that the broadening of linewidth for some Heusler films may originate from two-magnon scattering caused by crystallographic defects.[27,40] This may allow result in a perpendicular FMR linewidth lower than those of the

TABLE I. Magnetization and FMR parameters for a 180-Å-thick film of Co_2MnSb grown on GaAs (001).

$4\pi M_s = 10.8 \pm 0.2$ kG
$g = 2.08 \pm 0.01$
$K_1/M = -0.1747$ kOe
$K_\perp/M = 0.0142$ kOe
$K_1 = -150 \times 10^3$ erg/cm^3
$K_\perp = 12.18 \times 10^3$ erg/cm^3
FMR linewidth ΔH ($f = 9.55$ GHz):
$\Delta H = 130$ Oe, [110]
$\Delta H = 150$ Oe, [1$\bar{1}$0]
$\Delta H = 110$ Oe, [100]
$\Delta H = 380$ Oe, [001]

in-plane linewidths, close to the intrinsic value. However, in the present film, the out-of-plane FMR linewidth is larger than that of the in-plane orientation. We assume that the large out-of-plane linewidth is related to the strain state of the film.

Introducing the measured values above to Eqs. (4)–(6), we obtain the parameters $K_\perp = 12.18 \times 10^3$ erg/cm^3, $K_1 = -150 \times 10^3$ erg/cm^3, $\gamma' = 2.912 \pm 0.005$, and $g = 2.08 \pm 0.01$, which are comparable to those reported for the Co_2MnSi and Co_2MnGe film systems.[35] Note that these parameters were extracted assuming the in-plane uniaxial anisotropy K_u to be negligible due to the slight difference in magnetization values measured between the [110] and [1$\bar{1}$0] directions. Parameters derived from FMR and VSM measurements are listed in Table I.

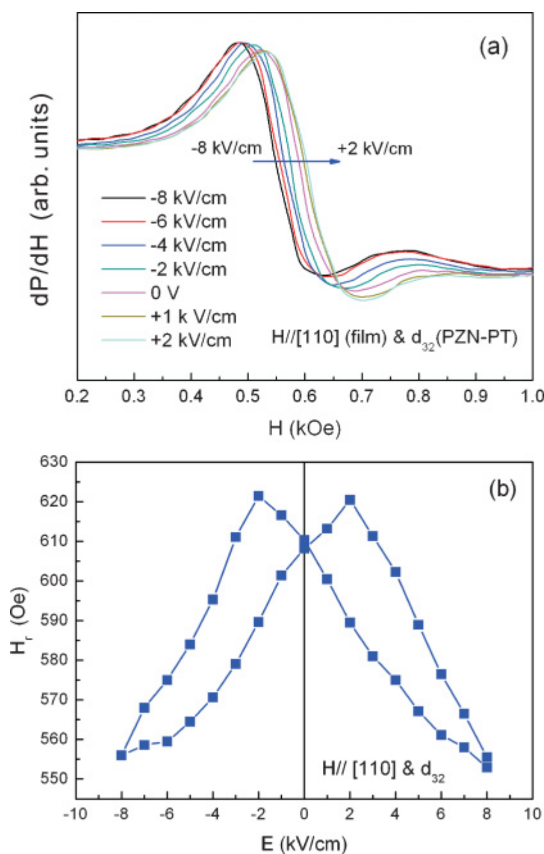

FIG. 7. (Color online) (a) FMR absorption derivatives as a function of magnetic field at different electric fields. (b) Tuning of the FMR field by an electric field across the PZN-PT crystal, while an applied magnetic field is aligned along the [110] direction of the film and the d_{32} direction of the PZN-PT crystal.

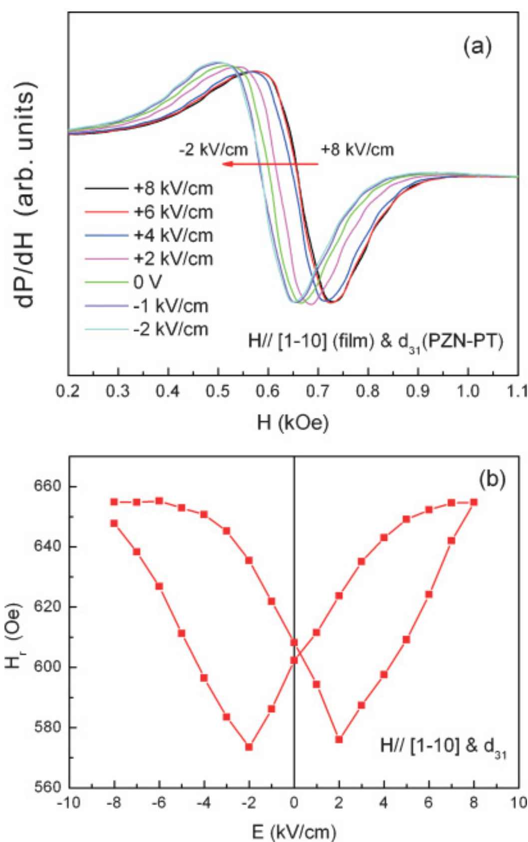

FIG. 8. (Color online) (a) Variation of FMR absorption derivative with magnetic field for different electric-field strengths. (b) FMR field as a function of electric-field strength applied across the PZN-PT crystal, while an applied magnetic field is aligned along the [1$\bar{1}$0] direction of the film and the d_{31} direction of the PZN-PT crystal.

C. Microwave magnetoelectric coupling

From the standpoint of both fundamental physics and MIC applications, an emphasis is placed on the microwave tunability of this MF heterostructure. Figure 7(a) shows the tuning of the FMR spectra under the application of an electric field. Figure 7(b) shows that the ferromagnetic resonance field (H_r) shifts clearly toward lower fields, which reflects an effective stress-induced magnetic field (δH_E) along the direction of the external magnetic field. It is understood that the orientation of the induced magnetic field is determined by the minimization of the magnetoelastic energy. The magnetoelastic energy can be expressed as $-\frac{3}{2}\lambda\sigma\cos^2\varphi$, where φ is the angle between the stress (σ) and magnetization (M) vectors. When λ and σ are of the same sign, i.e., $(\lambda\sigma) > 0$, M aligns along φ (=0) to minimize energy. That is, an equivalent stress-induced magnetic field is aligned with σ. This is the case for the d_{32} (>0) direction while the magnetostrictive coefficient was measured to be positive. The electric field facilitates a decrease in the resonance field, which

yields a maximum shift of 85–90 Oe with a sweep from $E=+8$ kV/cm-2 kV/cm. The decrease in the external magnetic field is compensated with an increase in the stress-induced internal magnetic field. Additionally, the H_r vs E curve displays the familiar butterfly shape [Fig. 7(b)], which is attributed to the correlation between strain and electric field. It is widely accepted that the appearance of a peak in the resonance field is related to the electronic coercivity of the PZN-PT crystal. Alternatively, the irreversible strain arising with electric field results from the ferroelectric hysteresis phenomenon, which is also presented for the PZN-PT crystal in Fig. 4. Therefore, it is reasonable that the two peaks in the external magnetic field appear near the coercive electric fields $E_c \approx 4$ kV/cm. This can be understood by examining the conversion of the electric field to magnetic field as a two-step process: First, an electric field generates the mechanical deformation of the PZN-PT crystal, and second, the PZN-PT strain is then communicated to the magnetostrictive film, inducing an internal magnetic field.

Similarly, when an applied magnetic field is aligned parallel to d_{31} (<0), the induced magnetic field remains aligned along d_{31} since $(\lambda\sigma)<0$, as shown in Fig. 8(a). In this case, the FMR field increases with the applied electric field strength, as shown in Fig. 7(b). This behavior arises from an additional torque on spins since the induced magnetic field is transverse to the external magnetic field.[41]

As presented above in Figs. 7 and 8, the E-field dependence of the FMR field shift is complicated, depending upon the history of electric polarization, while an external magnetic field is aligned parallel to the direction of either d_{31} or d_{32}. This reveals a near-linear correlation between E field and resonance-field shift over a wide range of electric-field strengths -2 and $+8$ kV cm^{-1}. A maximum δH_σ^E of 88 Oe results from a tuning of 10 kV cm^{-1}, indicating a magnetoelectric coupling coefficient A of 8.8 Oe cm kV^{-1}. Since this layered structure has a small magnetic filling factor we assume the strain to be transferred uniformly throughout the Heusler film. The strain-induced internal magnetic field can then be expressed as[42]

$$\delta H_\sigma^E = \frac{3\lambda\sigma}{M} = AE, \tag{13}$$

where A is the converse magnetoelectric constant and λ and σ are the magnetostriction constant and stress of the Co_2MnSb film, respectively. The stress inside the Heusler layer is expressed as $\sigma = E(d_{31}C_{11} + d_{32}C_{12})$, where the elastic moduli of the magnetic film are $C_{11} = 1.52 \times 10^{12}$ dyn/cm^2 and $C_{12} = 1.43 \times 10^{12}$ dyn/cm^2.[43] Thus, the stress-induced magnetic field is estimated to be $\delta H_\sigma^E \approx 100$ Oe, where $\lambda=11$ ppm, $d_{31} = -2700$ pC/N, $d_{32} = 1100$ pC/N, $E=10$ kV/cm, and $M=860$ G. This estimated value is comparable to the measured value of $\sim$88 Oe. The slight discrepancy may be attributed to the effective coupling between the PZN-PT crystal and the Co_2MnSb film due to the bending of the GaAs substrate in response to stress and/or the relatively small Young's modulus of the employed epoxy.[44]

Note that we can rewrite the stress-induced anisotropy constant in Eq. (9) by using the applied electric field (E) such that

$$K_\sigma^E = \tfrac{3}{2}\lambda\sigma = \tfrac{3}{2}\lambda E(d_{31}C_{11} + d_{32}C_{12}). \tag{14}$$

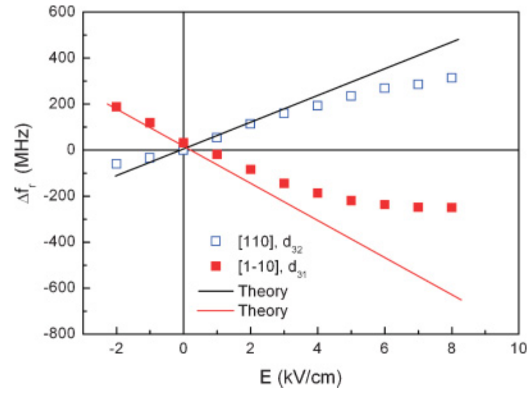

FIG. 9. (Color online) Variation of FMR frequency with applied electric-field strength for the Co_2MnSb/GaAs/PZN-PT heterostructure. Solid and hollow symbols denote the measured values, whereas the solid lines represent the theoretical prediction.

An equivalent stress-induced anisotropy constant K_σ^E is estimated to be 378 erg/cm^3, corresponding to $E=10$ kV/cm^3. Additionally, based on the theoretical model presented in Sec. II, the electric-field-tuned resonance shift can be calculated from Eqs. (11) and (12). Since the present film does not give rise to significant in-plane uniaxial anisotropy, K_u is reasonably ignored to simplify the calculation. Thus, when a magnetic field is aligned along d_{32} of the PZN-PT crystal, and **M** and **H** align along the [110] direction of the Co_2MnSb film, i.e., **H**//[110], $\varphi=\pi/4$ the resonance condition can be expressed as

$$\left(\frac{f}{\gamma'}\right)^2 = \left(H_r + \frac{2K_\sigma^E}{M} - \frac{2K_1}{M}\right) \times \left(H_r + \frac{2K_\sigma^E}{M} + 4\pi M - \frac{2K_\perp}{M} + \frac{K_1}{M}\right), \tag{15}$$

while for **H**//[1$\bar{1}$0], $\varphi=-\pi/4$, we obtain

$$\left(\frac{f}{\gamma'}\right)^2 = \left(H_r - \frac{2K_\sigma^E}{M} - \frac{2K_1}{M}\right) \times \left(H_r + 4\pi M - \frac{2K_\perp}{M} + \frac{K_1}{M}\right). \tag{16}$$

By taking $K_\perp = 12.18 \times 10^3$ erg/cm^3 and $K_1 = -150 \times 10^3$ erg/cm^3, the E-field dependence of the FMR frequency shift is illustrated in Fig. 9, indicating frequency shifts as large as 380 MHz along [110] and 440 MHz along [1$\bar{1}$0] under the application of $E=10$ kV/cm. Correspondingly, this represents a microwave tunablity of 38 MHz cm/kV along the d_{32} direction and 44 MHz cm/kV along the d_{31} direction. The electric-field dependence of the resonance frequency shift shows a linear relationship over a range of the electric field -2 to $+5$ kV/cm, which is of particular significance for practical device applications. It is noteworthy that these results are comparable to those reported in other bilayer structures[45] (e.g., 3–15 MHz cm kV^{-1} for YIG/PMN-PT), and trilayer structures [e.g., 15 MHz cm kV^{-1} for YIG/GGG/PMN-PT (Ref. 46) and 0.3–1 MHz cm kV^{-1} for YIG/BSTO/GGG (Ref. 47), where YIG, GGG and BSTO stand for yttrium iron garnet, gadolinnium gallium garnet and barium strontium

titanate, respectively]. However, the experimental data deviate somewhat from the theoretical predictions, plotted as the solid line in Fig. 9. Nonlinearity of either strain vs E field or the piezomagnetic effect may be contributing factors for this discrepancy.

Additionally, we notice that in Fig. 4 an abrupt change of the electric polarization at the coercive field results in an abrupt strain of the piezoelectric crystal. As a rule, an abrupt change in strain always accompanies the electric coercive field, although there are different shapes of P-E curves for various piezoelectric crystals. We point out that the strain may give rise to an abrupt change in magnitude or even a change in sign near the coercive field.[48] Importantly, the ME effect or FMR shift is acutely sensitive to the increase or decrease in strain at E=0, as is the case when the electric field is swept through the coercive field. It leads to the result that the shift in the resonance field changes sign (i.e., relative to the H_r value at E=0) in the range of electric fields between −2 and +2 kV/cm, as presented in Figs 7(b) and 8(b). Note that at the coercive field there are usually pronounced peaks of strain in response to the electric field. In brief, the tuning behavior of the magnetic anisotropy field or the FMR shift is completely consistent with the field dependence of strain in a piezoelectric or magnetostrictive material. Ideally, the magnetostrictive material should have the same strain behavior as the piezoelectric crystal under the application of an electric field. The efficiency of ME coupling has been recently discussed theoretically.[49] It is expected to result in highly efficient and low-consumption magnetoelectric devices.

V. CONCLUSIONS

In summary, we report a large linear electric-field tuning of the microwave ferromagnetic resonance frequency in a Co_2MnSb/GaAs/PZN-PT multiferroic heterostructure, indicating a microwave tunability of ∼44 MHz cm kV^{-1} and a converse magnetoelectric coupling coefficient A of 8 Oe cm kV^{-1}. A theoretical model was derived and used to explain and predict the ferromagnetic resonance behavior under the application of an electric field for this class of heterostructures. The demonstration of microwave tuning of a MF heterostructure based on a GaAs substrate provides a valuable pathway to realizing future applications in multifunctional microwave integrated circuits.

ACKNOWLEDGMENTS

This work was supported by the National Science Foundation under Grant No. G00003249. S.S. would like to acknowledge support from the National Science Foundation (Grant No. NSF-DMR-0545728).

*Corresponding author: y.chen@neu.edu

†Present address: Department of Physics, University of Alberta, Canada.

[1] M. I. Bichurin, D. Viehland, and G. Srinivasan, J. Electroceram. **19**, 243 (2007).

[2] M. Fiebig, J. Phys. D **38**, R123 (2005).

[3] C. W. Nan, M. I. Bichurin, S. Dong, and D. Viehland, J. Appl. Phys. **103**, 031101 (2008).

[4] W. Eerenstein, N. D. Mathur, and J. F. Scott, Nature (London) **442**, 759 (2006).

[5] F. Zavaliche, T. Zhao, H. Zheng, F. Straub, M. P. Cruz, P.-L. Yang, D. Hao, and R. Ramesh, Nano Lett. **7**, 1586 (2007).

[6] Y. Chen, T. Fitchorov, C. Vittoria, and V. G. Harris, Appl. Phys. Lett. **97**, 052502 (2010).

[7] G. Srinivasan and Y. K. Fetisov, Integr. Ferroelectr. **83**, 89 (2006).

[8] Y. Chen, T. Fitchorov, A. L. Geiler, J. S. Gao, C. Vittoria, and V. G. Harris, Appl. Phys. A **100**, 1149 (2010).

[9] S. Dong, J. Zhai, J. Li, and D. Viehland, Appl. Phys. Lett. **89**, 252904 (2006).

[10] Y. Chen, A. L. Geiler, T. Fitchorov, C. Vittoria, and V. G. Harris, Appl. Phys. Lett. **95**, 182501 (2009).

[11] A. L. Geiler, S. M. Gillette, Y. Chen, J. Wang, Z. Chen, S. D. Yoon, P. He, J. Gao, C. Vittoria, and V. G. Harris, Appl. Phys. Lett. **96**, 053508 (2010).

[12] E. H. Gregory, Microwave J. **30**, 119 (1987).

[13] Y. Chen, J. Gao, J. Lou, M. Liu, S. D. Yoon, A. L. Geiler, M. Nedoroscik, D. Heiman, N. X. Sun, C. Vittoria, and V. G. Harris, J. Appl. Phys. **105**, 07A510 (2009).

[14] Y. Chen, J. Gao, D. Heiman, C. Vittoria, and V. G. Harris, J. Phys. D **43**, 495002 (2010).

[15] Y. Chen, D. Basiaga, J.R. O'Brien, and D. Heiman, Appl. Phys. Lett. **84**, 4301 (2004).

[16] B. Ravel, J. O. Cross, M. P. Raphael, V. G. Harris, R. Ramesh, and V. Saraf, Appl. Phys. Lett. **81**, 2812 (2002)

[17] M. P. Raphael, B. Ravel, Q. Huang, M. A. Willard, S. F. Cheng, B. N. Das, R. M. Stroud, K. M. Bussmann, J. H. Claassen, and V. G. Harris, Phys. Rev. B **66**, 104429 (2002).

[18] B. Ravel *et al.*, Phys. Rev. B **65**, 184431 (2002).

[19] M. Raphael, B. Ravel, M. A. Willard, S. F. Cheng, B. N. Das and V. G. Harris, Appl. Phys. Lett. **79**(26), 4396 (2001).

[20] M. Overby, A. Chernyshov, L. P. Rokhinson, X. Liu, and J. K. Furdyna, Appl. Phys. Lett. **92**, 192501 (2008).

[21] T. Ambrose, J. J. Krebs, and G. A. Prinz, J. Appl. Phys. **87**, 5463 (2000).

[22] B. Heinrich, J. F. Cochran, M. Kowalewski, J. Kirschner, Z. Celinski, A. S. Arrott, and K. Myrtle, Phys. Rev. B **44**, 9348 (1991).

[23] C. Vittoria, *Magnetics, Dielectrics, and Wave Propagation with* MATLAB *Codes* (CRC Press, Boca Raton, FL, 2010), Chap. 5.

[24] M. Farle, B. Mirwald-Schulz, A. N. Anisimov, W. Platow, and K. Baberschke, Phys. Rev. B **55**, 3708 (1997).

[25] B. Schulz and K. Baberschke, Phys. Rev. B **50**, 13467 (1994).

[26] X. Liu, Y. Sasaki, and J. K. Furdyna, Phys. Rev. B **67**, 205204 (2003).

[27] B. Heinrich, G. Woltersdorf, R. Urban, O. Mosendz, G. Schmidt, P. Bach, L. Molenkamp, and E. Rozenberg, J. Appl. Phys. **95**, 7462 (2004).

[28] B. Heinrich, S. T. Purcell, J. R. Dutcher, K. B. Urquhart, J. F. Cochran, and A. S. Arrott, Phys. Rev. B **38**, 12879 (1988).

[29] C. Vittoria, H. Lessoff, and N.D. Wilsey, IEEE Trans. Magn. **8**, 273 (1972).

[30]M. Farle, Rep. Prog. Phys. **61**, 755 (1998).
[31]M. R. Paudel, C. S. Wolfe, N. Ali, S. Stadler, J. A. Christodoulides, D. L. Ederer, Y. Li, T. A. Callcott, and J. W. Freeland, J. Appl. Phys. **105**, 103907 (2009).
[32]S. Stadler *et al.*, J. Appl. Phys. **97**, 10C302 (2005).
[33]M. Liu, O. Obi, J. Lou, Y. Chen, Z. Cai, S. Stoute, M. Espanol, M. Lew, X. Situ, K. S. Ziemer, V. G. Harris, and N. X. Sun, Adv. Funct. Mater. **19**, 1826 (2009).
[34]K.K. Rajan, M. Shanthi, W.S. Chang, J. Jin, and L.C. Lim, Sens. Actuators, A **133**, 110 (2007).
[35]Y. Chen, T. Fitchorov, Z. Cai, K. S. Ziemer, C. Vittoria, and V. G. Harris, J. Phys. D **43**, 155001 (2010).
[36]C. Thiele, K. Dörr, O. Bilani, J. Rödel, and L. Schultz, Phys. Rev. B **75**, 054408 (2007) .
[37]M. Belmeguenai, F. Zighem, Y. Roussigné, S-M. Chérif, P. Moch, K. Westerholt, G. Woltersdorf, and G. Bayreuther, Phys. Rev. B **79**, 024419 (2009).
[38]D. Serratea, J. M. De Teresaa, R. Córdobaa, and S. M. Yusufa, Solid State Commun. **42**, 363 (2007).
[39]S. Trudel, O. Gaier, J. Hamrle, and B. Hillebrands, J. Phys. D **43**, 193001 (2010).
[40]C. Vittoria, S. D. Yoon, and A. Widom, Phys. Rev. B **81**, 014412 (2010).
[41]F. Y. Yang, C. H. Shang, C. L. Chien, T. Ambrose, J. J. Krebs, G. A. Prinz, V. I. Nikitenko, V. S. Gornakov, A. J. Shapiro, and R. D. Shull, Phys. Rev. B **65**, 174410 (2002).
[42]R. C. O'Handley, *Modern Magnetic Materials—Principles and Applications* (John Wiley & Sons, NewYork, 2000).
[43]J. Worgull, E. Petti, and J. Trivisonno, Phys. Rev. B **54**, 15695 (1996).
[44]Y. Chen, J. Wang, M. Liu, J. Lou, N. X. Sun, C. Vittoria, and V. G. Harris, Appl. Phys. Lett. **93**, 112502 (2008).
[45]G. Srinivasan, A. S. Tatarenko, V. Mathe, and M. I. Bichurin, Eur. Phys. J. B **71**, 371 (2009).
[46]S. Shastry G. Srinivasan, M. I. Bichurin, V. M. Petrov, and A. S. Tatarenko, Phys. Rev. B **70**, 064416 (2004).
[47]J. Das, Y.-Y. Song, N. Mo, P. Krivosik, and C. E. Patton, Adv. Mater. **21**, 2045 (2009).
[48]A. Amin, E. McLaughlin, H. Robinson,and L. Ewart, IEEE Trans. Ultrason. Ferroelectr. Freq. Control **54**, 1090 (2007).
[49]M. I. Bichurin, V. M. Petrov, and G. Srinivasan, J. Appl. Phys. **92**, 7681 (2002)